Nanotechnology **19** (2008) 245606 (7pp) doi:10.1088/0957-4484/19/24/245606

Fabrication of silicon carbide nanowires/carbon nanotubes heterojunction arrays by high-flux Si ion implantation

Huaping Liu[1], **Guo-An Cheng, Changlin Liang and Ruiting Zheng**

Key Laboratory of Radiation Beam Technology and Material Modification of Education Ministry, Department of Materials Science and Engineering, Institute of Low Energy Nuclear Physics, Beijing Normal University, Beijing Radiation Center, Beijing 100875, People's Republic of China

E-mail: lhp77616@tom.com and gacheng@bnu.edu.cn

Received 23 February 2008, in final form 8 April 2008
Published 9 May 2008
Online at stacks.iop.org/Nano/19/245606

Abstract

An array of silicon carbide nanowire (SiCNW)–carbon nanotube (CNT) heterojunctions was fabricated by high-flux Si ion implantation into a multi-walled carbon nanotube (MWCNT) array with a metal vapor vacuum arc (MEVVA) ion source. Under Si irradiation, the top part of a CNT array was gradually transformed into an amorphous nanowire array with increasing Si dose while the bottom part still remained a CNT structure. X-ray photoelectron spectroscopy (XPS) analysis shows that the SiC compound was produced in the nanowire part even at the lower Si dose of 5×10^{16} ions cm^{-2}, and the SiC amount increased with increasing the Si dose. Therefore, the fabrication of a SiCNW–CNT heterojunction array with the MEVVA technique has been successfully demonstrated. The corresponding formation mechanism of SiCNWs was proposed.

1. Introduction

SiC nanowires have a bright future in the field of electronic nanodevices operating in high temperature, high frequency and high power conditions due to their excellent chemical inertness, high thermal conductivity, high breakdown field and excellent field emission properties [1–4]. Therefore, various methods have been developed to synthesize SiC nanowires, including chemical vapor deposition (CVD) [4], laser ablation [5], carbothermal reduction [6, 7], arc discharge [8], etc. However, among these preparation methods, the high synthesis temperature of SiC nanowires is required, which hindered their large-scale production and industrial application.

Ion beam synthesis (IBS) of SiC has been widely used because of its precise control of implantation dose and excellent reproducibility [9–13]. Another attractive feature of IBS is the capability of forming SiC at relatively low temperatures. However, IBS using the conventional IBS technique suffers in general from the long implantation time because of the high-dose requirement, which has prevented the development of studies on the formation kinetics of SiC by IBS. To overcome this problem, the metal vapor vacuum arc (MEVVA) ion source has been developed [14], which has broad-beam and high-current capabilities. The MEVVA source uses the principle of vacuum arc discharge between the cathode and the anode to create a dense plasma of cathode material and hence an intense ion beam of the cathode material is extracted. The MEVVA ion source operates in a pulse mode which can lead to very high instantaneous input power density during implantation, and a mean current of tens of mA can be obtained. Therefore, based on the one-dimensional shape of CNTs, Si implantation into the as-prepared CNT arrays with a MEVVA ion source seems to be a promising technique for the large-scale fabrication of SiC nanowires.

In this work, we report the fabrication of SiCNW–CNT heterojunction arrays by Si ion implantation into the as-

[1] Present address: Department of Physics, Tokyo University of Science, Shinjuku, Tokyo 162-8601, Japan.

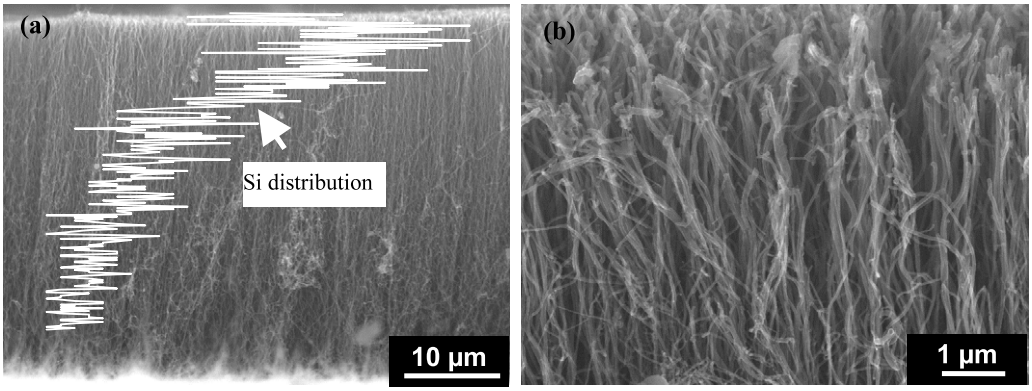

Figure 1. FESEM images of the as-implanted CNTs with Si dose of 2×10^{17} ions cm^{-2} and the corresponding Si depth profile in the CNT array. (a) Side view of the as-implanted CNT arrays, (b) close-up view of the CNT array top. The line plot along the height of the CNT film in (a) is the EDX spectrum of the Si element.

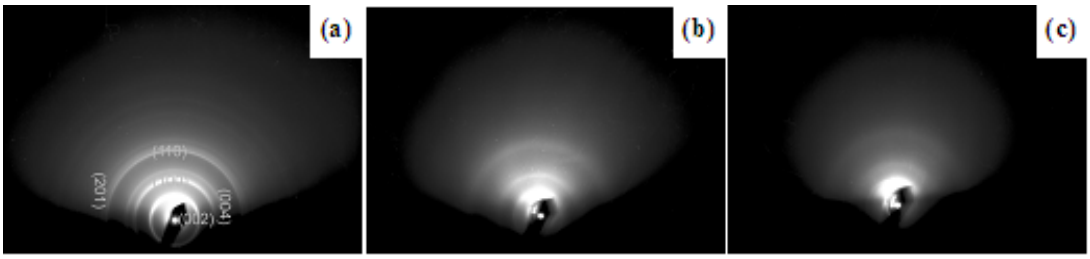

Figure 2. RHEED images of the as-implanted CNT films with different doses of Si ions. (a) 0 ions cm^{-2}, (b) 5×10^{16} ions cm^{-2} and (c) 2×10^{17} ions cm^{-2}.

prepared CNT arrays at low temperature using the MEVVA ion source technology. We investigated the structure and composition change of CNTs, and discussed the formation mechanism of SiC nanowires under Si ion irradiation.

2. Experimental details

The CNT arrays used in our experiment were synthesized with a thermal chemical vapor deposition method. The detailed process can be found in our previous paper [15]. The IBS of SiC nanowires/CNT heterojunction arrays was performed by high-flux Si ion implantation into the as-grown CNT arrays at an energy of 40 keV at doses of 1×10^{16}, 5×10^{16}, 1×10^{17} and 2×10^{17} ions cm^{-2} using the home-made MEVVA ion source, which was typically operated at a pulse width of the order of 1.2 ms and a pulse interval of 0.3–1.0 s. The resistivity of Si source materials used as the cathode was 10^{-3} Ω cm. During implantation, the average substrate temperature was about 230 °C because of the ion beam heating effect, which can be measured by a thermocouple attached to the Si substrate. The working pressure was around 2×10^{-3} Pa.

The morphologies and structures of CNTs before and after Si implantation were characterized by scanning electron microscopy (SEM), reflection high-energy electron diffraction (RHEED) and high-resolution transmission electron microscopy (HRTEM). The Si atom concentration depth profile in the as-implanted CNT films was analyzed by energy-dispersive x-ray spectroscopy (EDX). X-ray photoelectron spectroscopy (XPS) was used to characterize the chemical bonding state of Si and C in the as-implanted CNT arrays.

3. Results and discussion

Typical SEM images of the as-implanted CNT array with the Si dose of 2×10^{17} ions cm^{-2} (figure 1) reveal that the as-implanted CNT arrays still remained the array morphology. The higher magnification of the as-implanted CNT array top (figure 1(b)) clearly shows that the diameters of the CNT tips expanded. The Si depth profile measured by EDX in the as-implanted CNT films (figure 1(a)) indicates that the maximum intensity of the Si element is located near the array top. Similar results were observed at implantation doses of 5×10^{16} and 1×10^{17} ions cm^{-2}. However, we did not find the clear expansion effect of the nanotube diameter at a dose of 1×10^{16} ions cm^{-2}.

In order to investigate the effects of Si ion implantation on the graphite structures of CNT films, we analyzed the CNT films before and after implantation by employing the RHEED technique. Before implantation, the clear electron diffraction rings imply (figure 2(a)) that the as-grown CNTs had good graphitic structures. However, after implantation the electron diffraction rings became ambiguous even at the lower dose of 5×10^{16} ions cm^{-2} (figure 2(b)). On increasing the dose to 2×10^{17} ions cm^{-2}, the electron diffraction rings of CNT structures almost disappear (figure 2(c)). These results demonstrate that the implantation damage was produced under

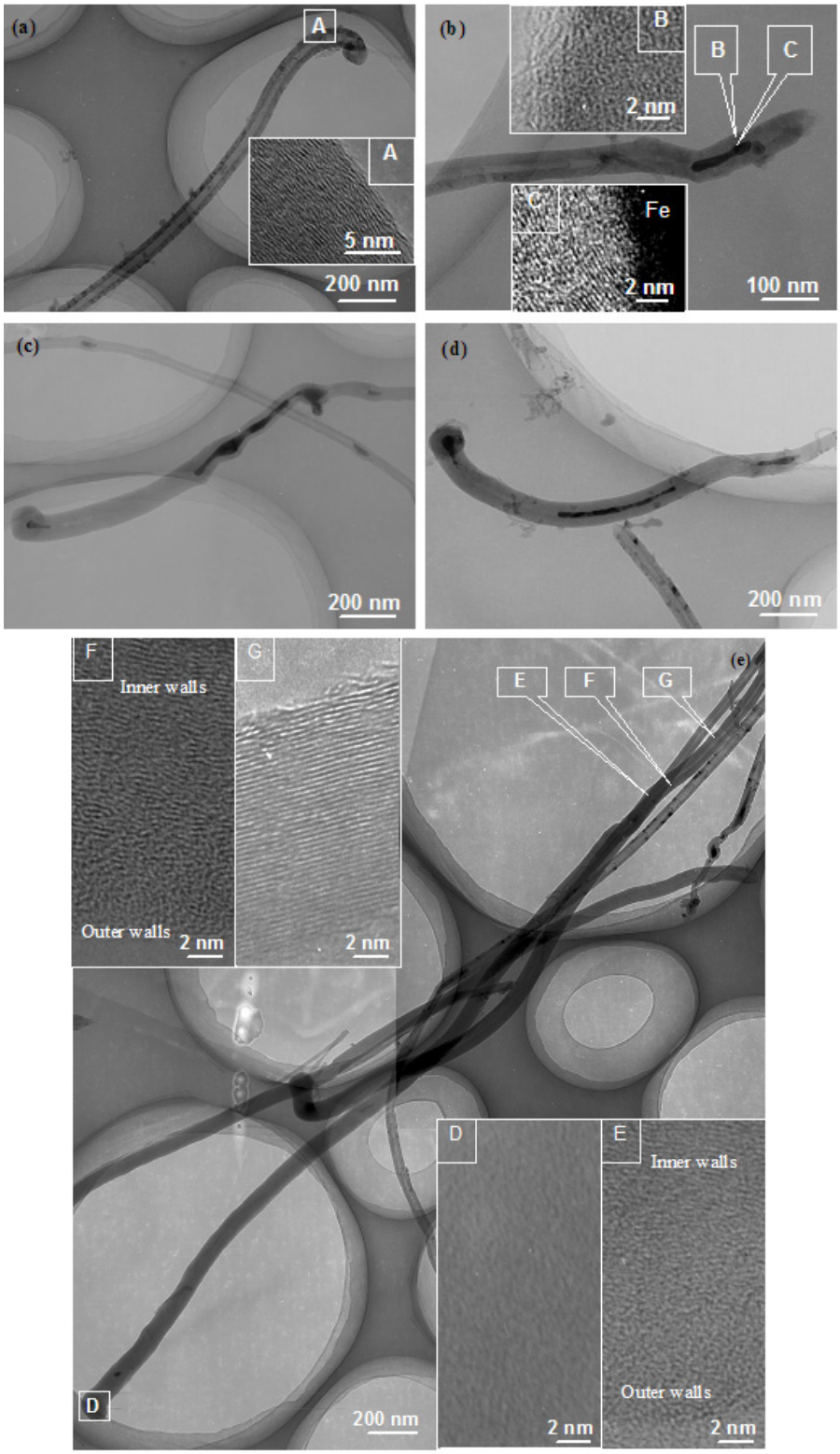

Figure 3. TEM and HRTEM images of single CNTs before and after Si implantation with different doses. (a) An as-grown CNT, (b) 1×10^{16} ions cm^{-2}, (c) 5×10^{16} ions cm^{-2}, (d) 1×10^{17} ions cm^{-2} and (e) 2×10^{17} ions cm^{-2}. Insets A–G are the corresponding high magnification of parts A–G indicated in the nanotubes.

the irradiation of Si ions, and the damage degree increased with increasing the Si dose.

Typical TEM images of a single CNT before and after implantation with different Si doses are shown in figure 3. As you can see, the as-grown CNTs have a hollow structure (figure 3(a)) with well-ordered graphitic sheets (part A in figure 3(a)). After Si implantation with the dose of 1×10^{16} ions cm^{-2}, the outer walls of the CNT tips were damaged

and the bent and disordered graphitic sheets can be seen (part B in figure 3(b)) while the inner walls still remained well-ordered graphitic-layer structures (part C in figure 3(b)). Therefore, the tubular shape of the CNT tips was not destroyed (figure 3(b)). On increasing the Si dose to 5×10^{16} ions cm^{-2}, the inner walls of the CNT tips were damaged and the tube structures collapsed, and about 800 nm long CNT tips were transformed into amorphous nanowires (ANWs) with a uniform diameter and a smooth surface (figure 3(c)). On continuously increasing the Si ion dose to 1×10^{17} ions cm^{-2}, the nanowire length increased to about 2 μm (figure 3(d)). At the dose of 2×10^{17} ions cm^{-2} about 4 μm long nanowires were observed (figure 3(e)). From figures 3(c)–(e), another attractive feature is that the diameters of the as-formed nanowires expanded about 50–100% compared with the corresponding CNT diameters when the Si dose was higher than 5×10^{16} ions cm^{-2}. The outer diameter of the transition from nanowire part to nanotube part decreases gradually, whereas the inner diameters increase (figure 3(e)).

The atomic structure change of individual CNTs after implantation along their length is shown in parts D–G in figure 3(e), which clearly exhibit the formation process of nanowires under Si irradiation. Part D shows that no graphitic sheets can be seen in the nanowire part and small particles or clusters were seemingly formed while the nanotube part still has good graphitic-crystal structure (Part G). Parts E and F reveal that the number of well-ordered graphitic sheets increases gradually in the transition part from nanowire to nanotube. Also the corresponding outer walls are composed of disordered graphitic sheets, which are similar to the structures of the outer walls of the CNT tips irradiated at the Si dose of 1×10^{16} ions cm^{-2} (part B in figure 3(b)). These results sufficiently demonstrate that the damage of CNTs was gradually produced from outer walls to inner walls and from the top down the height of the CNT arrays under Si irradiation.

During the ion bombardment, the CNTs are subject to structural change due to displacement collisions and collision cascade effects, which generate large quantities of defects (vacancies and interstitials) in the tube walls. The concentration of higher defects results in the increment of the degree of disorder, and the well-ordered graphitic sheets of CNTs break into local ordered graphite. As the irradiation dose increases, more defects are generated. Continued generation of defects makes the CNTs collapse and form ANWs with a uniform diameter and a smooth surface, as shown in figures 3(c)–(e). At the same time, the creation of large amounts of vacancies and interstitials and the distortion of graphitic sheets in implantation leads to the expansion of the as-formed ANW diameters [16, 17]. The atomic structure change along the CNT length under Si irradiation means that the different areas along the CNT length receive different doses under a nominal irradiation dose due to the implantation depth of the incident ion beam in CNT films. The CNT tips evolved into ANWs because of receiving more doses, whereas the transition from nanowire part to nanotube part became an amorphous nanotube because of receiving a lower irradiation dose. Also no structural change occurred for the nanotube root part due to no actual ion irradiation.

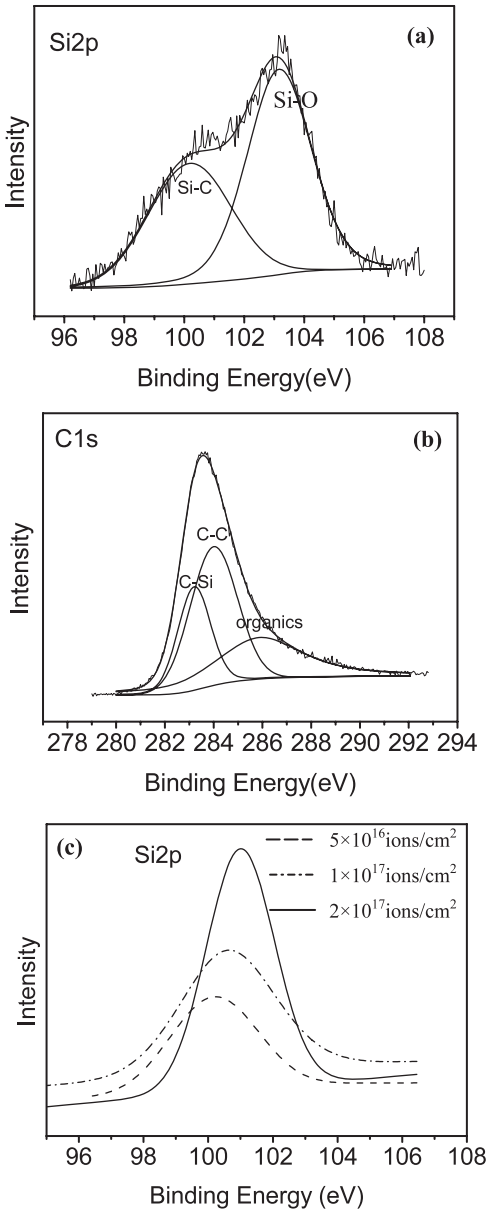

Figure 4. (a) Si 2p and (b) C1s peaks of XPS spectra of nanotubes implanted with the dose of 5×10^{16} ions cm^{-2}. (c) The Si 2p peaks corresponding to SiC formed in the as-implanted with different doses: 5×10^{16}, 1×10^{17} and 2×10^{17} ions cm^{-2}.

The chemical state of C and Si elements in CNT films after Si implantation was characterized using XPS. Figure 4 shows the XPS analysis results of CNT films after Si implantation with the dose of 5×10^{16} ions cm^{-2}. The broad and asymmetrical Si 2p peak (figure 4(a)) indicates that the chemical state of the Si element is not single. We obtained the two peaks at 100.3 and 103.2 eV by peak fitting. We assigned the Si 2p peak at 100.3 eV to Si–C covalent bonds and the peak at 103.2 eV to Si–O covalent bonds in SiO_2. The formation of SiO_2 is possibly related to the low vacuum. The signal derived from SiO_2 on Si substrates is another factor that influences the results during XPS measurement. C 1s also has a broad and asymmetrical peak (figure 4(b)). After peak fitting, we found that the C1s peak was superimposed by three peaks, which

were located at 283.2 eV, 284.2 eV and 285.9 eV, respectively. They should correspond to the C 1s peaks in SiC, graphite and organic compounds, which could result from the diffusion pump in the vacuum system. These results demonstrate that SiC was formed after Si ion implantation even with the lower dose of 5×10^{16} ions cm^{-2}.

Similar results were obtained in the case of 1×10^{17} ions cm^{-2} and 2×10^{17} ions cm^{-2}. The Si 2p peaks of the SiC compounds formed at different doses are integrated in figure 4(c), which shows that the intensity of the Si 2p signal corresponding to Si–C bonds increases and the corresponding binding energy shifts towards higher binding energies with increasing Si dose. When the Si ion dose increased to 2×10^{17} ions cm^{-2}, the Si 2p peak moved to about 101.00 eV. The corresponding full width at half-maximum (FWHM) of the Si 2p peaks also varied as the Si dose was increased. From figure 4(c), we know the FWHM of the Si 2p peaks is 3.25 eV, 3.48 eV and 2.75 eV for doses of 5×10^{16} ions cm^{-2}, 1×10^{17} ions cm^{-2} and 2×10^{17} ions cm^{-2}, respectively.

An increase in the Si 2p peak intensity of Si–C bonds with increasing Si implantation dose implies that more Si–C bonds were formed under higher Si dose. The shift of the corresponding Si 2p binding energy with increasing Si dose indicates the change in the chemical state of the silicon atoms. As the silicon atoms are bound to the carbon atoms in the implanted samples, the charge transfer from the silicon atoms to the more electronegative carbon atoms leads to the shift of the Si 2p peaks towards higher binding energy [12]. When the Si dose was increased to 2×10^{17} ions cm^{-2}, the Si 2p binding energy attained a value of about 101.00 eV, which is close to that of silicon bonded to carbon in β-SiC (101.00) [18]. Therefore, the observed intensity increase and shift of the Si 2p peak of Si–C bonds on increasing the Si dose suggest that Si–C bonds are more easily formed on increasing the Si dose. This is understood if one considers that the probability of the carbon atoms bound to the Si atoms is expected to become greater when the silicon dose increases because of the higher concentration of implanted Si ions in the CNT films.

Figure 4(c) also shows that the FWHM of the Si 2p peak varied with increasing Si dose. According to the mechanism of XPS, the FWHM of Si 2p peaks is determined by the monochromaticity of the x-rays, the detection range of the detector and the degree of order around Si atoms. Under the same monochromaticity of x-ray and detection range of the detector, the higher the degree of order is, the narrower the FWHM of Si 2p peaks is. Therefore, the FWHM changes of the Si 2p peak with the implantation dose reflects the relationship between the degree of order around the implanted Si atoms and the Si atom concentration. Although SiC compounds were fabricated under low dose, the implanted Si alloyed by carbon resulted in an increase in the disorder of the bonding structures and the implantation damage effect [12, 19–22]. Therefore, the corresponding Si 2p peak had a larger FWHM on increasing the Si dose from 5×10^{16} ions cm^{-2} to 1×10^{17} ions cm^{-2}. Similar broadening in the width of the Si 2p signal with increasing carbon content was observed in previous works [12, 21]. With the Si dose continuously increased to 2×10^{17} ions cm^{-2}, the reduction in the width of the Si 2p signal indicates that SiC clusters with higher degree of order have been formed in nanowires at the high-dose implantation.

The fabrication of SiC by carbon implantation into Si materials with a MEVVA ion source has been reported [12, 13]. However, they did not discuss the formation process of C–Si bonds in detail. Here we would like to clarify the formation mechanism of SiC compounds by a non-equilibrium mechanism during the implantation process. As mentioned above, the MEVVA ion source provided a pulsed Si ion beam. The pulse width was 1.2 ms and the pulse interval was 0.3–1.0 s. During the implantation, the implanted Si ions triggered a series of atomic collisions among the implanted Si ions and the target C atoms. According to atomic collision theory, such a process is usually divided into two steps, i.e. atom collision and a relaxation immediately after atom collision, which lasts for a very short time period of 10^{-10}–10^{-9} s. Clearly, the pulse interval is much longer than the relaxation time period. Having these figures in mind, we divide each pulsed Si ion implantation into three steps.

The first step is atom collision (1.2 ms). The high-energy Si ions were dynamically launched into the carbon lattice in CNT films where they simultaneously triggered dramatic atom collisions between Si and C atoms, resulting in the dislocation of C atoms and the formation of a highly energetic Si and C mixture. It is commonly recognized that, during this step, the SiC compound cannot be formed because these atoms are in violent motion.

The second step is relaxation (10^{-10}–10^{-9} s). In the second step of relaxation, beginning at the termination of atom collisions, the bombarded but not dislocated carbon atoms would vibrate at their equilibrium positions. If the energy is released in the form of thermal energy, a global thermal spike centered at the thermal source would be formed. The thermal spikes would expand in the form of macro-thermodynamics with increasing time obeying the following thermal conductance formula [23]:

$$\nabla T = \frac{1}{D}\frac{\partial T}{\partial t} \tag{1}$$

where D is thermal diffusivity, its relationship to thermal conductivity C, heat capacity c, and density ρ being

$$D = \frac{C}{c\rho}. \tag{2}$$

Assuming the environmental temperature T_0, when one thermal source Q appears at one point in CNT films at $t = 0$, the solution to formula (1) is

$$T(\gamma, t) = T_0 + \frac{Q}{(4\pi)^{2/3} c\rho}\frac{1}{(Dt)^{3/2}}\exp\left(-\frac{\gamma^2}{4Dt}\right). \tag{3}$$

In the formula, $C = 650$–830 W m^{-1} K^{-1} [24], $c = 0.51$ KJ Kg^{-1} K^{-1}, $\rho = 1.31$ g cm^{-3}, and γ is the distance from the thermal source. Q is the thermal energy of one thermal source. Usually we do not consider the temperature distribution at $t = 0$. The dislocation threshold energy of the C atoms in multi-walled CNTs is $E_d \approx 15$–20 eV [25], and

that in amorphous carbon is $E_d \approx 5$ eV [26] or 10 eV [27]. Therefore, the vibrational energy of the bombarded carbon atoms in the CNT lattice would possibly reach about 15 eV, and that of carbon atoms in amorphous carbon can reach 5 eV. According to the calculation of the above formula, if the vibrational energy is completely transformed into thermal energy, 15 eV energy can make the temperature within a globe with a diameter of 10 Å increase to more than 1400 °C, and in the case of 5 eV the temperature of the globe with 10 Å diameter can also reach about 1000 °C. As we know, the reaction temperature between C and Si solid phases usually is 1000–1400 °C [28, 29]. In our experiment the Si atoms were incorporated into CNT films by implantation instead of thermal diffusion or chemical potential, which made it possible that the Si atoms stayed in CNT films bound to the carbon atoms around them at considerably lower temperatures than that required in the reaction between C and Si solid phases. Therefore, the temperature is high enough to form SiC compounds. However, the volume of the globe with 10 Å diameter is very small. On the other hand, the implanted Si atoms are usually located in the environment with the rich carbon atoms and are separated by the carbon atoms. Therefore, only one or several SiC molecules can be formed in such a small volume, and these SiC molecules might be isolated. With increasing time, the temperature decreases rapidly and the highly energetic Si + C mixture relaxes towards equilibrium. After 10^{-10}–10^{-9} s, the temperature approaches the environmental temperature. The as-formed SiC compounds are usually amorphous because the short time limited the atomic diffusion. Clearly, it was during the non-equilibrium physical process that the SiC compounds were formed.

The third step is defined as the time period from the end of the above relaxation to the next implantation pulse (0.3–1.0 s). The implantation of high-energy Si ions into CNT films induced high-density defects, especially vacancies. These vacancies diffuse in the part under irradiation and continuously recover with the interstitial atoms or the dislocations, and finally reach dynamic equilibrium. Thus, a stable vacancy field might be formed from the surface to the inside. During the third step, the as-grown SiC compounds should undergo a random diffusion driven by the vacancy field, and possibly organize themselves to form clusters. If the SiC clusters can grow into a sufficiently large size before the arrival of the next implantation pulse, they would not be smashed completely by the impact of the incoming Si ions, and can remain in the nanowire part. When the next pulse arrives, some new SiC compounds could be formed and the growth of the previously retained SiC clusters could continue to proceed.

The continuation of the above three processes results in the formation of a continuous SiC cluster network in the irradiated nanowire part. With increasing Si ion dose, more and more Si ions bond to C atoms, resulting in an increase in SiC compound density and the growth of SiC clusters. At the same time, an increase in the Si dose also increases the synthesis time of SiC compounds, which is helpful for the diffusion of SiC molecules, and hence the growth and reorganization of SiC clusters. Therefore, the increasing of Si dose might increase the order degree of SiC compounds, which has been demonstrated by the XPS results. However, the crystallization of SiC is still difficult because of the low synthesis temperature.

4. Conclusions

We have performed Si implantation into the as-grown CNT arrays with a MEVVA ion source. Under Si irradiation, the top part of the CNT arrays were transformed into amorphous SiC nanowires when the dose was sufficiently high while the bottom part still remained as CNT structures. Therefore, the fabrication of SiCNW–CNT heterojunction arrays at low temperatures by the MEVVA technique was demonstrated. IBS with a MEVVA ion source opens up a new way to synthesize large-scale compound nanowires at low temperature. Although only amorphous nanowires have been fabricated, their crystallization can possibly be achieved by heat treatment at high temperature. Therefore, the SiCNW–CNT heterojunction arrays fabricated with a MEVVA ion source have a potential for application in rectifying diodes, light-emitting diodes, and so forth, after further heat treatment.

Acknowledgment

This work is supported by the National Natural Science Foundation of China (NSFC, grant no. 10575011).

References

[1] Wong E W, Sheehan P E and Lieber C M 1997 *Science* **277** 1971
[2] Zhou W M, Liu X and Zhang Y F 2006 *Appl. Phys. Lett.* **89** 223124
[3] Pan Z W *et al* 2000 *Adv. Mater.* **12** 1186–90
[4] Wong K W, Zhou X T, Frederick C K, Lai H L, Lee C S and Lee S T 1999 *Appl. Phys. Lett.* **75** 2918–20
[5] Shi W, Zheng Y, Peng H, Wang N, Lee C S and Lee S T 2000 *J. Am. Ceram. Soc.* **83** 3228–30
[6] Hu J Q, Lu Q Y, Tang K B, Deng B, Jiang R R, Qian Y T, Yu W C, Zhou G E, Liu X M and Wu J X 2000 *J. Phys. Chem.* B **104** 5251–4
[7] Gao Y H, Bando Y, Kurashima K and Sato T 2001 *Scr. Mater.* **44** 1941–4
[8] Seeger T, Redlich P and Rühle M 2000 *Adv. Mater.* **12** 279–82
[9] Marin P, Daudin B, Dupuy M, Ermolieff A, Olivier M, Papon A M and Rolland G 1990 *J. Appl. Phys.* **67** 2908
[10] Reeson K J, Stoemenos J and Hemment P L F 1990 *Thin Solid Films* **191** 147
[11] Nejim A, Hemment P L F and Stoemenos J 1995 *Appl. Phys. Lett.* **66** 2646–8
[12] Han Y, Kwok R W M and Wong S P 1996 *Appl. Surf. Sci.* **92** 61–5
[13] Han Y, Kwok R W M and Wong S P 1996 *Diamond Relat. Mater.* **5** 556–9
[14] Brown I G, Gavin J E and MacGill R A 1985 *Appl. Phys. Lett.* **47** 358–60
[15] Liu H P, Cheng G A, Zhao Y, Zheng R T, Liang C L, Zhao F and Zhang T H 2006 *Surf. Coat. Technol.* **201** 938–42
[16] Kim H M, Kim H S, Park S K, Joo J, Lee T J and Lee C J 2005 *J. Appl. Phys.* **97** 026103

[17] Sun L T, Gong J L, Wang Z X, Zhu D Z, Hu J G, Lu R R and Zhu Z Y 2005 *Nucl. Instrum. Methods Phys. Res.* B **228** 26–30
[18] Kitabatake M, Deguchi M and Hirao T 1993 *J. Appl. Phys.* **74** 4438–45
[19] Morimoto A, Miura T, Kumeda M and Shimizu T 1982 *J. Appl. Phys.* **53** 7299–305
[20] Morimoto A, Oozra S, Kumeda M and Shimizu T 1983 *Solid State Commun.* **47** 773–7
[21] Takeshita T, Kurata Y and Hasegawa S 1992 *J. Appl. Phys.* **71** 5395–400
[22] Ni Z C, Li Q T, Gong J L, Zhu D Z and Zhu Z Y 2007 *Nucl. Instrum. Methods Phys. Res.* B **260** 542–6
[23] Dienes G J and Vineyard G H 1957 *Radiation Effects in Solids* (New York: Interscience)
[24] Choi T Y, Poulikakos D, Tharian J and Sennhauser U 2005 *Appl. Phys. Lett.* **87** 013108
[25] Banhart F, Foiler T, Redlich P and Ajayan P M 1997 *Chem. Phys. Lett.* **269** 349–55
[26] Cosslett V E 1978 *J. Microsc.* **113** 113–29
[27] Banhart F 1999 *Rep. Prog. Phys.* **62** 1181–221
[28] Liu J W, Zhong D Y, Xie F Q, Sun M, Wang E G and Liu W X 2001 *Chem. Phys. Lett.* **348** 357–60
[29] Larciprete R, Lizzit S, Cepek C, Botti S and Goldoni A 2003 *Surf. Sci.* **532–5** 886–91